12th IFAC International Symposium on
Advanced Control of Chemical Processes
July 14-17, 2024. Toronto, Canada

Stabilizing extremum seeking control applied to model-free bioprocess productivity optimization

Laurent Dewasme * **Alain Vande Wouwer** *

* *Systems, Estimation, Control and Optimization (SECO) , University of Mons, 7000 Mons, Belgium (e-mail: <laurent.dewasme, alain.vandewouwer>@umons.ac.be).*

Abstract: This study investigates an application of stabilizing extremum seeking (STAB-ESC) to model-free bioprocess productivity optimization. To this end, microbial growth in a chemostat is considered as a typical example. In contrast with the classical ESC formulation, STAB-ESC confines the measurable cost function in the argument of a periodic and bounded control function, which confers very interesting features to the control scheme in terms of sparse parameter tuning, fast convergence and robustness to measurement noise. These points are highlighted in the present study through an analysis of the Lie-bracket average dynamics and a performance comparison with a Newton-based recursive ES.

Keywords: Data-driven control, stabilization, optimization, averaging, process control.

1. INTRODUCTION

Extremum seeking control (ESC) is a direct output feedback adaptation scheme that allows finding the optimum of a steady-state cost function. The seminal ESC version of Ariyur and Krstic (2003), inspired by the work of Leblanc (1922), is model-free and only requires a measurable cost function whose gradient estimate will be forced towards zero, as shown in Figure 1.

In the past 20 years, ESC has received ever-increasing attention, and many applications (mostly simulations) have been reported. Tan et al. (2010) presented a very thorough review of the literature related to model-free ESC, while more recently, we (Dewasme and Vande Wouwer, 2020) provided a closer look at ESC applications to bioprocesses. Indeed, bioprocesses are characterized by the difficulty of establishing reliable models in a context where uncertainties are prevalent. ESC can alleviate this difficulty by a direct optimization of a measurable objective function, without resorting to a process model.

However, the main drawback of ESC is the time-scale separation induced by the gradient estimator dynamics which must be slower than the process. While this issue worsens in the case of multiple inputs, it is also obviously affected by slow (bio)process dynamics (Dewasme et al., 2017). Several ways for accelerating the gradient estimation have been proposed in recent years, for instance using a Wiener-Hammerstein representation (Moase and Manzie, 2012), or using recursive estimators (Guay, 2015). Both solutions have been combined by Feudjio Letchindjio et al. (2019) to optimize the productivity of microalgae cultures, validated by a successful experimental implementation (Feudjio Letchindjio et al., 2021). Guay and Dochain (2017) also proposed to add a proportional action to the classical integrator, leading to a so-called proportional-integral extremum seeking control (PIESC) to accelerate the response transient. Newton-based methods have also been investigated to take advantage of the Hessian estimate in the optimization (Moase et al., 2010; Ghaffari et al., 2012; Dewasme and Vande Wouwer, 2022).

Other recent studies focus on fixed-time convergence (Poveda and Krstic, 2021; Guay, 2020, 2021), and the possibility of connecting extremum seeking control with Lyapunov functions (Sontag, 1989), using averaging to develop a new framework of model-free stabilizing ESC denoted STAB-ESC (Scheinker and Krstić, 2017; Labar et al., 2019, 2022). STAB-ESC operates as a high-gain controller in contrast to the classical ESC of Figure 1 and offers interesting guaranteed bounds on the input update rate by confining the measured cost function in the argument of a sin/cos dither signal. In addition to remarkable robust properties, STAB-ESC has a natural noise-rejecting convergence.

The main motivation of this work is to investigate the use of STAB-ESC in the context of bioprocess applications, and its robustness to measurement noise.

This paper is organized as follows: section 2 briefly presents a generic bioprocess model. Section 3 reviews the STAB-ESC main properties and design guidelines while section 4 illustrate the behavior of the method as compared to the recursive Newton-based method presented in (Dewasme and Vande Wouwer, 2022). Conclusions are drawn in section 5.

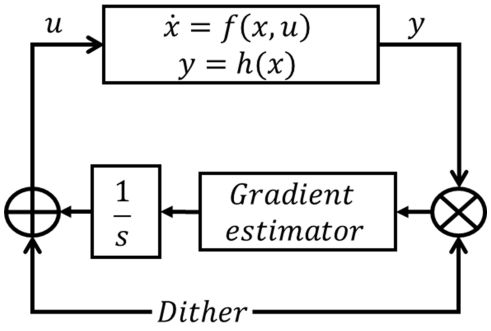

Fig. 1. Classical extremum seeking scheme (Ariyur and Krstic, 2003).

2. BIOPROCESS DESCRIPTION

As a worked example, we consider a generic microbial growth model which describes the typical dynamic behavior of a con-

tinuous cell culture, growing on a specific substrate with activation/saturation kinetics represented by a Monod law.

2.1 Microbial growth model

The reaction scheme reads:

$$k_s S \rightarrow X \tag{1}$$

where X and S are respectively standing for the biomass and substrate, while k_s is the substrate yield coefficient. A continuous operation of the culture is considered, maintaining the bioreactor volume V constant by equal inlet and outlet feed rates F. The corresponding dilution rate is assumed to be the sole manipulated input $u = \frac{F}{V}$. Applying mass balance to (1) yields the following ordinary differential equation system representing the species concentration dynamics:

$$\dot{x} = \mu x - u x \tag{2a}$$
$$\dot{s} = -k_s \mu x - u(s - s_{in}) \tag{2b}$$

where x and s are, respectively, the concentrations of biomass and substrate, and s_{in} is the inlet substrate concentration. The specific reaction rate is modeled by the following Monod law:

$$\mu = \frac{\mu_{max} s}{K_s + s} \tag{3}$$

where μ_{max} is the maximum rate parameter, K_s is the half-saturation constant, and the corresponding reaction rate is $\varphi = \mu X$.

The productivity $J = u\,x$ is the performance index, where x is assumed to be measurable and, in turn, also J. This measurable index is the output of the system, also written:

$$y = ux \tag{4}$$

A bifurcation analysis, developed in Wang et al. (1999), shows that the non-wash-out steady-state is defined and remains stable as long as the steady-state input $u_{ss} < \frac{s_{in}\,\mu_{max}}{s_{in} - K_s}$.

3. BOUNDED EXTREMUM SEEKING FOR UNKNOWN MAP

3.1 Modified extremum seeking

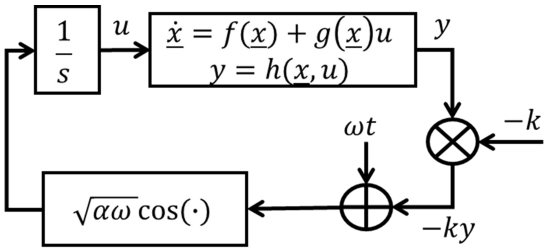

Fig. 2. Bounded stabilizing extremum seeking.

We consider a generic form of (2), which is an input-affine nonlinear system expressed as follows:

$$\dot{\underline{x}} = f(\underline{x}) + g(\underline{x})u \tag{5}$$

where $\underline{x} \in \mathbb{R}^{+,n}$ is the state vector, $f, g : \mathbb{R}^{+,n} \rightarrow \mathbb{R}^n$ are general nonlinear functions and $u \in \mathbb{R}^+$ is the single input. We restrict this study to a single-input-single-output (SISO) case where the output (4) is also expressed in a generic form, i.e. $y \in R^+$, with

$$y = h(\underline{x}, u) \tag{6}$$

where $h : \mathbb{R}^{+,n+1} \rightarrow \mathbb{R}^+$, is the nonlinear output function.

Stabilizing extremum seeking of unknown map considers the inclusion of a cost function J, assumed to be a cost Lyapunov function (CLF), in the argument of a bounded periodic dither input signal of the form:

$$\dot{u} = \sqrt{\alpha\,\omega}\,cos\,(\omega\,t - k\,J) \tag{7}$$

where ω is the pulsation of the periodic signal (7), α and k are parameters which, a priori, are respectively used to tune the magnitude and the argument of (7). In the following, the CLF J is assumed to be the measurable output y of the system, i.e. $J = h(\underline{x}, u)$, and there exists an optimal input value u^* such that:

$$\nabla J(\pi(u^*), u^*) = 0 \; and \; \nabla J \neq 0 \; \forall u \neq u^* \tag{8}$$

where $\pi(u) : \mathbb{R}^+ \rightarrow \mathbb{R}^{+,n}$ is the equilibrium map of the state variables. The resulting closed-loop system is shown in Figure 2.

It should be noticed that the form of (7) allows bounding the input variations depending only on the argument of the *cos* function.

3.2 Weak limit for averaging

To study the dynamics of the stabilizing ESC, the average closed-loop trajectory is commonly computed to approximate the solution of the actual periodically disturbed system (Khalil, 2002). This approximation is represented by the average of (7) when considering a small parameter ε. This equation can be rewritten after rescaling time in $\tau = \omega t$ and setting $\varepsilon = \frac{1}{\omega}$ as in (Dürr et al., 2013):

$$\frac{du}{d\tau} = \frac{\sqrt{\alpha\omega}}{\omega} cos(\tau - kJ) = \varepsilon(\frac{\sqrt{\alpha}}{\sqrt{\varepsilon}} cos(\tau - kJ)) = \varepsilon f(\tau, u, \varepsilon) \tag{9}$$

Applying averaging to system (9) is therefore impossible due to the presence of the factor $\frac{1}{\sqrt{\varepsilon}}$ in f (averaging requires that $f(\tau, u, 0)$ exists).

Therefore, a Lie bracket averaging analysis is used instead, based on the definition of a weak limit. For the sake of clarity, we review the main results of Scheinker and Krstić (2017) and, more particularly, theorem 2.3 applied to (7), which we first expand as follows, renaming each factor as h_1, b_1, h_2 and b_2:

$$\dot{u} = \underbrace{\sqrt{\alpha\,\omega}\,cos\,(\omega\,t)}_{h_1}\,\underbrace{cos\,(k\,J)}_{b_1} + \underbrace{\sqrt{\alpha\,\omega}\,sin\,(\omega\,t)}_{h_2}\,\underbrace{sin\,(k\,J)}_{b_2} \tag{10}$$

The averaging step consists of finding a way to compute (10) when ω tends to infinity, using the concept of weak limits. Studying the weak limit of h_1 and h_2 requires the use of the *Riemann-Lebesgue* Lemma which states that, for a function $f(x)$ defined on a compact set C of the Lebesgue-integrable space (i.e., $L^1(C)$),

$$\lim_{\omega \rightarrow \infty} \int_C f(x) e^{-i\omega x} dx = 0 \tag{11}$$

and a sequence of functions $f_k \subset L^2[0,1]$ is said to weakly converge to f, denoted $f_k \rightharpoonup f$, if

$$\lim_{k \rightarrow \infty} \int_0^1 f_k(\tau) g(\tau) d\tau = \int_0^1 f(\tau) g(\tau) d\tau, \forall g \in L^2[0,1] \tag{12}$$

It is easily proven that h_1 and h_2 have uniform and weak limits, respectively written:

$$\lim_{\omega\to\infty}\int_{t_0}^{t} h_i\, d\tau = 0\ \forall i \tag{13a}$$

$$h_i \int_{t_0}^{t} h_j\, d\tau \rightharpoonup \lambda_{i,j} \tag{13b}$$

where $\rightharpoonup$ means "weak limit" (Scheinker and Krstić, 2017), and

$$\sqrt{(\alpha\omega)}cos(\omega t)\int_{t_0}^{t}\sqrt{(\alpha\omega)}cos(\omega\tau)\,d\tau \rightharpoonup \lambda_{1,1}=0 \tag{14a}$$

$$\sqrt{(\alpha\omega)}cos(\omega t)\int_{t_0}^{t}\sqrt{(\alpha\omega)}sin(\omega\tau)\,d\tau \rightharpoonup \lambda_{1,2}=-\frac{\alpha}{2} \tag{14b}$$

$$\sqrt{(\alpha\omega)}sin(\omega t)\int_{t_0}^{t}\sqrt{(\alpha\omega)}cos(\omega\tau)\,d\tau \rightharpoonup \lambda_{2,1}=\frac{\alpha}{2} \tag{14c}$$

$$\sqrt{(\alpha\omega)}sin(\omega t)\int_{t_0}^{t}\sqrt{(\alpha\omega)}sin(\omega\tau)\,d\tau \rightharpoonup \lambda_{2,2}=0 \tag{14d}$$

We now consider the integral by parts of the products b_i by h_i and obtain:

$$\begin{aligned}&\lim_{\omega\to\infty}\int_{t_0}^{t} b_i(u,\tau)h_i(\tau)d\tau\\ &=\lim_{\omega\to\infty}\left[b_i(u,\tau)|_{t_0}^{t}\int_{t_0}^{t}h_i(\tau)d\tau-\int_{t_0}^{t}\frac{db_i(u,\tau)}{d\tau}\int_{t_0}^{t}h_i(r)dr\,d\tau\right]\end{aligned} \tag{15}$$

The first term vanishes following (13a) and the second term can be expanded as:

$$\begin{aligned}&\lim_{\omega\to\infty}\int_{t_0}^{t}\frac{\partial b_i(u,\tau)}{\partial\tau}\int_{t_0}^{t}h_i(r)dr\,d\tau\\ &+\lim_{\omega\to\infty}\sum_{j=1}^{2}\int_{t_0}^{t}\frac{\partial b_i(u,\tau)}{\partial u}b_j(u,\tau)h_j(\tau)\int_{t_0}^{t}h_i(r)dr\,d\tau\end{aligned} \tag{16a}$$

$$=\sum_{i\neq j}\int_{t_0}^{t}\frac{\partial b_i(\bar{u},\tau)}{\partial u}b_j(\bar{u},\tau)\lambda_{i,j}(t)d\tau \tag{16b}$$

The first term in (16a) vanishes due to (13a) and the second term yields (16b) in view of (14). Considering the dynamics of expression (16b), i.e., without the integral from t_0 to t, the average system or Lie-bracket system of (10) can be written:

$$\dot{\bar{u}}=\frac{\partial b_1}{\partial u}b_2\lambda_{1,2}+\frac{\partial b_2}{\partial u}b_1\lambda_{2,1} \tag{17}$$

where $\bar{u}$ stands for the average input trajectory. Combining (14) and (17) leads to:

$$\dot{\bar{u}}=\frac{k\,\alpha}{2}\nabla J \tag{18}$$

The proposed extremum seeking loop (10) uniformly converges to the trajectory (18) such that the optimum u^* is $\frac{1}{\omega}$-SPUAS (semiglobally practically uniformly asymptotically stable; see (Moreau and Aeyels, 2000; Scheinker and Krstić, 2017) for further details). This uniform asymptotic stability is valid for a sufficiently large value of ω, i.e. there exists a lower bound ω_L such that the results hold for any $\omega > \omega_L$. It also appears that α and k can be used to tune the convergence rate. k can therefore be considered as a gain while α allows tuning both the periodic signal magnitude and the convergence rate. ω, k and α should be taken sufficiently large, resulting in a high-gain extremum seeking loop, conversely to the classical ESC.

4. NUMERICAL RESULTS

The simulation study first compares the performances of STAB-ESC and the Newton-based block-oriented model strategy described in (Dewasme and Vande Wouwer, 2022), which is briefly sketched in Figure 3.

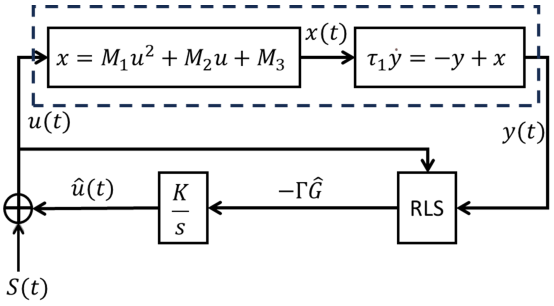

Fig. 3. Newton-based block-oriented model extremum seeking scheme. The process (dotted box) is assumed to be represented by a Hammerstein model.

The Newton-based extremum seeking (NS) strategy assumes that the process can be described by a Hammerstein model, i.e., a static nonlinear relation between the state $x(t)$ and the input $u(t)$, followed by a first-order linear dynamic relation between $x(t)$ and the output $y(t)$. A recursive least square algorithm estimates the parameters of both the static and dynamic blocks, i.e., M_1, M_2, M_3 and τ_1, and delivers an estimate of the gradient $\hat{G}=\frac{\partial\hat{y}}{\partial u}$ multiplied by the estimate of the inverse Hessian Γ. This is achieved under the assumption of a persistent excitation from the dither signal $S(t)$ of the form:

$$S(t) = A_1 sin(\omega_1 t) + A_2 sin(\omega_2 t) \tag{19}$$

where $A_{1,2}$ and $\omega_{1,2}$ are respectively the magnitudes and pulsations of the dither signal. The presence of two sinusoidal terms ensures the identifiability of the 4 unknown parameters. The closed-loop dynamic equations derived from Figure 3 read:

$$\dot{\hat{u}} = -K\Gamma\hat{G} \tag{20a}$$

$$u = \hat{u} + S(t) \tag{20b}$$

$$\dot{\tilde{\theta}} = -R^{-1}\varphi\varphi^T\tilde{\theta} \tag{20c}$$

$$\dot{R} = \varphi\varphi^T - \lambda R \tag{20d}$$

where R is the information matrix (the inverse covariance matrix), φ is the regressor, λ is the forgetting factor, θ stands for the unknown parameter vector and $\tilde{\theta}=\hat{\theta}-\theta$ is the parameter estimation error ($\hat{\theta}$ being the parameter estimate). More details on this strategy can be found in (Dewasme and Vande Wouwer, 2022).

4.1 Nominal performance analysis

In the following, we consider the parameter values of model (2) given in Table 1 and the parameters of the ESC schemes in Table 2.

The selection of the NS parameter values aims at providing a fair performance comparison and, therefore, the fastest achievable convergence for the chosen initial conditions $x(0) = 1\ g/L$, $s(0) = 9\ g/L$ and $u(0) = 0.2\ h^{-1}$. While the NS strategy follows classical extremum seeking tuning rules such as a small integrator gain and slow dither frequencies (scaled lower than the process dynamics), the STAB-ESC is tuned as a high-gain controller, i.e. with high gain k and dither frequency ω.

A parameter design sequence is required to tune the STAB-ESC convergence rate and, in turn, the closed-loop dynamics. The pulsation ω is first chosen with a few limitations in mind. Indeed, an ordinary differential equation (ODE) solver is used

to numerically solve the dynamic model equations (2) and the control law (7). Depending on the choice of the solver, a variable or fixed integration step could be defined. Considering T_s as the maximum time step (which can be set by the user, imposing successive solver calls over a T_s time span), ω should therefore be chosen sufficiently high with respect to an a priori unknown lower bound ω_L, but also so as to satisfy the Shannon theorem related to T_s, i.e., $\omega < \frac{1}{2}\,\omega_s$ where $\omega_s = \frac{2\,\pi}{T_s} \approx 60\ h^{-1}$). A reasonable choice is therefore made with $\omega = 24\ h^{-1}$. It should be noticed that during practical studies on a true plant, T_s can also be considered as the sampling time.

The gain k and magnitude α are then designed in the wake of ω, such that their respective orders of magnitude are not chosen too big with respect to ω. This rule results from dynamic changes induced by k and α when the ODE solver presents varying time steps to compute the solutions of (2) and (7), which become less accurate as k and α increase. k is therefore set to 10 and $\alpha = \frac{0.01}{\omega}$ to provide small oscillation magnitude in (7), i.e. $\sqrt{\alpha\,\omega} = \sqrt{0.01}$. It should be noticed that α also influences the convergence rate and a trade-off with the oscillation magnitude must therefore be achieved. Regarding the NS ESC, the two components of the dither signal are designed at low frequencies with small magnitudes, while the forgetting factor is set to 0.8 to significantly take into account past errors. This design is chosen in accordance with classical ESC guidelines (Dewasme et al. (2011); Dewasme and Vande Wouwer (2022)). The gain K is however fairly set by trial and error, to obtain the best results.

A first practical advantage of STAB-ESC is the smaller number of parameters to tune (NS ESC has twice more parameters, i.e., 6 versus 3 for STAB-ESC), see Table 2).

The simulation results shown in Figures 4 and 5 highlight the good performance of STAB-ESC to control the bioprocess under consideration but also the faster convergence than NS ESC (note also the higher-frequency oscillations).

Table 1. Parameter values of model (2).

Parameter	*Value*	*Unit*
k_s	0.5	gs/gx
μ_{max}	1.4	h^{-1}
K_s	12	g/L
s_{in}	50	g/L

Table 2. Tuning of the ESC strategies.

NS			STAB-ESC		
Parameter	*Value*	*Unit*	*Parameter*	*Value*	*Unit*
K	0.007	-	k	10	$L\,h\,g^{-1}$
λ	0.8	-	-	-	-
ω_1	$\frac{2\,\pi}{50}$	h^{-1}	ω	24	$[h^{-1}]$
ω_2	$\frac{2\,\pi}{25}$	h^{-1}	-	-	-
A_1	0.02	h^{-1}	α	$\frac{0.01}{\omega}$	h^{-3}
A_2	0.01	h^{-1}	-	-	-

4.2 Robustness with respect to noise

An important feature of process control is the capability of handling disturbances. Measurement noise may be a limitation for most of the adaptive control techniques, including extremum seeking. Practically, measurement noise can be attenuated by low-pass filters which however also tend to slow down the closed-loop dynamics.

Interestingly, STAB-ESC shows an immune-to-noise convergence property. Indeed, considering the functions b_1 and b_2

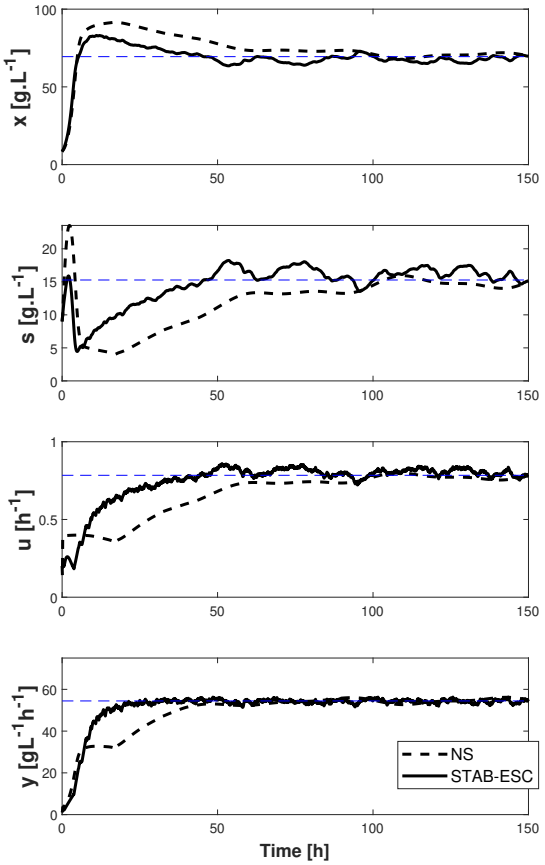

Fig. 4. Comparison of the performance of STAB-ESC (continuous black line) with the NS ESC (dashed black line): states, input u and output y evolutions. The blue dashed line shows the steady-state map optimum.

in (10) where J is now assumed to be corrupted by noise, i.e. $J = y + \varepsilon$ where ε is a white noise, b_1 can be expressed as:

$$b_1 = cos(k\,J)\ cos(\varepsilon) - sin(k\,J)\ sin(\varepsilon) \tag{21}$$

The Lie derivative in (17) can therefore be developed as:

$$\frac{\partial b_1}{\partial u} b_2 = -\frac{\partial J}{\partial u} sin^2(kJ + \varepsilon) \tag{22}$$

The same reasoning holds for b_2:

$$\frac{\partial b_2}{\partial u} b_1 = -\frac{\partial J}{\partial u} cos^2(kJ + \varepsilon) \tag{23}$$

such that (18) remains unchanged.

Despite the invariance in the average convergence behavior, STAB-ESC remains sensitive during the update stage when solving equation (7) and, to avoid entering a region too close to the wash-out equilibrium ($x = 0$ and $s = s_{in}$), a reduction of the parameter values should be considered. In the following, ω is reduced to 5, k to 4 and α to $\frac{0.0005}{\omega}$. For the same reasons, the NS ESC parameters are also revised to $K = 0.001$, and $\lambda = 0.2$ while the same dither signal is used.

A Monte Carlo study is achieved, considering 50 runs for each ESC scheme with the same initial conditions as in section

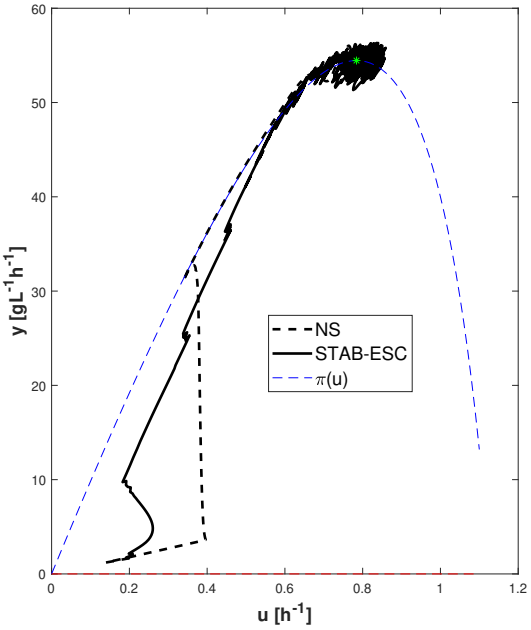

Fig. 5. Comparison of the performance of STAB-ESC (continuous black line) with NS ESC (dashed black line): convergence diagram. $\pi(u)$ represents the equilibrium map of the cost function y in dashed blue.

4.1 and white noise with zero mean and a relative standard deviation of 1 % corrupting the measurement of the cost function. Based on the current biomass probe technology level, this choice seems reasonable. However, the ESC parameters should be decreased as the noise level increases.

In Figures 6 and 7, STAB ESC displays a smooth and thin corridor of trajectories, testifying of the robust behavior with respect to measurement noise, even if the convergence is slowed down (the time axis of Figure 6 has been scaled). NS ESC still works but shows uneven performance with a larger average corridor of trajectories with some failures to converge to the correct optimum. This behavior may be linked to the violation of the general least square assumption that only the measurements are affected by noise but not the regressor. However, in the present formulation, the regressor uses the previous measurements as explanatory variables; see (Dewasme and Vande Wouwer, 2022). Figure 8 confirms the robust behavior of the STAB-ESC when the noise standard deviation is increased to 5 %. In this case, the parameterization is revised as $\omega = 3$, $k = 0.75$ and $\alpha = \frac{1.5\ 10^{-4}}{\omega}$.

5. CONCLUSION

This paper reports on the potential application of stabilizing extremum seeking to model-free bioprocess control. To this end, the productivity optimization of a generic continuous culture is considered, first in a noise-free ideal scenario, then in the more realistic situation where the measurable cost function is corrupted by noise. STAB-ESC provides fast convergence with great robustness to measurement noise, superseding other classical ESC schemes, as illustrated by a comparison with Newton seeking ESC.

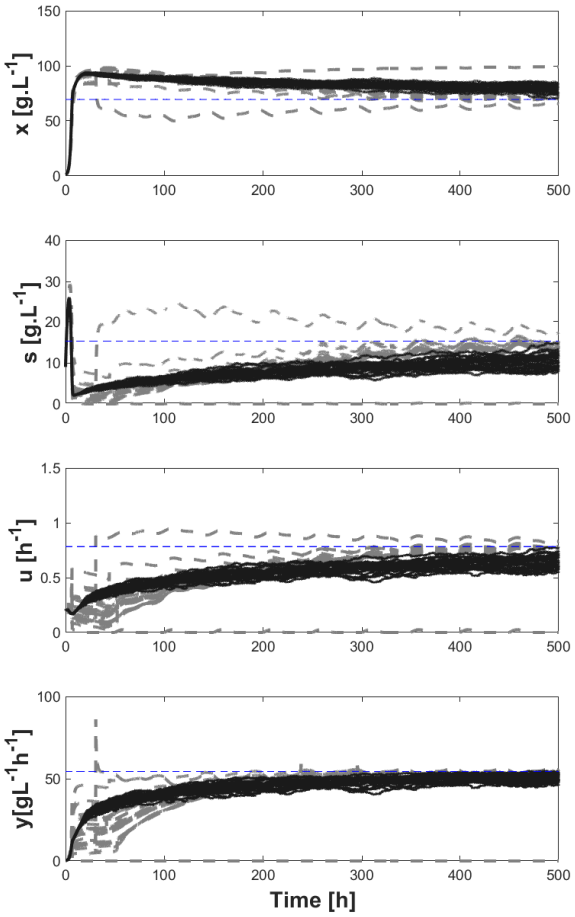

Fig. 6. Comparison of the performance of STAB-ESC (continuous black line) with NS ESC (dashed black line) in the presence of 1% measurement noise: states, input u and output y evolutions. The blue dashed line shows the steady-state map optimum.

STAB-ESC therefore appears as a solid strategy in practical cases, with an easier and more intuitive design combined with good robustness with respect to measurement noise as long as the parameterization is revised accordingly. Future perspectives concern its extension to fed-batch cases where the process does not reach a steady-state and where a specific exponential trajectory must be tracked (Dewasme et al. (2011)). Another important perspective is the experimental application of STAB-ESC to the microalgae plant described in Feudjio Letchindjio et al. (2021).

ACKNOWLEDGMENT

This research was supported by the European Union and Wallonia, under the European Regional Development Fund 2021-2027 program (DECARBOWAL portfolio/WalBioPower project).

REFERENCES

Ariyur, K.B. and Krstic, M. (2003). *Real-time Optimization by Extremum-seeking Control*. John Wiley & Sons, INC, Wiley-

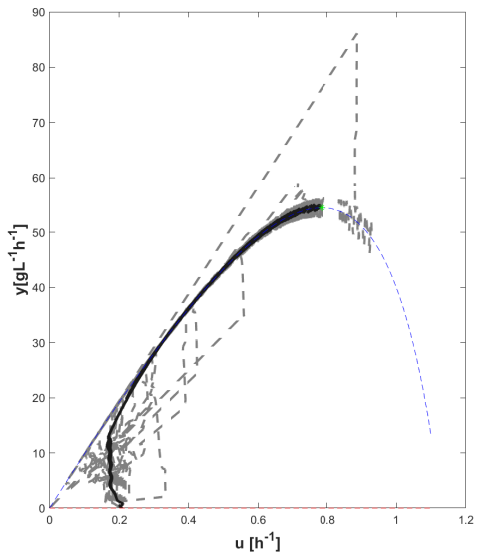

Fig. 7. Comparison of STAB-ESC (continuous black line) with NS ESC (dashed black line) in the presence of 1% measurement noise: convergence diagram. The equilibrium map of the cost function y is in dashed blue.

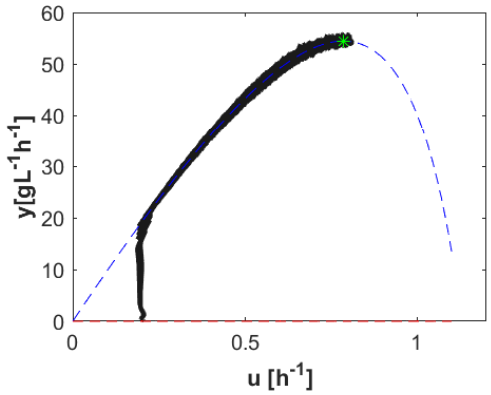

Fig. 8. STAB-ESC performance in the presence of 5% measurement noise: convergence diagram. The equilibrium map of the cost function y is in dashed blue.

Interscience edition.

Dewasme, L., Srinivasan, B., Perrier, M., and Vande Wouwer, A. (2011). Extremum-seeking algorithm design for fed-batch cultures of microorganisms with overflow metabolism. *J. Process Control*, 21(7), 1092–1104.

Dewasme, L. and Vande Wouwer, A. (2020). Model-free extremum seeking control of bioprocesses: A review with a worked example. *Processes*, 8(10), 1209.

Dewasme, L., Feudjio Letchindjio, C.G., Zuniga, I.T., and Vande Wouwer, A. (2017). Micro-algae productivity optimization using extremum-seeking control. In *2017 25th Mediterranean Conference on Control and Automation (MED)*, 672–677. IEEE.

Dewasme, L. and Vande Wouwer, A. (2022). Two simple model-free extremum seeking strategies with convergence acceleration through hessian estimation. In *2022 IEEE 61st Conference on Decision and Control (CDC)*, 2662–2667. IEEE.

Dürr, H.B., Stanković, M.S., Ebenbauer, C., and Johansson, K.H. (2013). Lie bracket approximation of extremum seeking systems. *Automatica*, 49(6), 1538–1552.

Feudjio Letchindjio, C.G., Dewasme, L., and Vande Wouwer, A. (2021). An experimental application of extremum seeking control to cultures of the microalgae scenedesmus obliquus in a continuous photobioreactor. *International Journal of Adaptive Control and Signal Processing*, 35(7), 1285–1297.

Feudjio Letchindjio, C.G., Dewasme, L., Deschênes, J.S., and Vande Wouwer, A. (2019). An extremum seeking strategy based on block-oriented models: Application to biomass productivity maximization in microalgae cultures. *Industrial and Engineering Chemistry Research*, 58(30), 13481–13494.

Ghaffari, A., Krstić, M., and Nesić, D. (2012). Multivariable newton-based extremum seeking. *Journal of Process Control*, 48, 1759–1767.

Guay, M. (2020). Finite-time newton seeking control for a class of unknown static maps. In *Proceedings of the IEEE Conference on Decision and Control*, 1435–1440.

Guay, M. (2015). Proportional-integral extremum-seeking control. *IFAC-PapersOnLine*, 48(8), 675–680.

Guay, M. (2021). Dual mode finite-time seeking control for a class of unknown dynamical system. *IFAC-PapersOnLine*, 54(3), 31–36.

Guay, M. and Dochain, D. (2017). A proportional-integral extremum-seeking controller design technique. *Automatica*, 77, 61–67.

Khalil, H. (2002). *Nonlinear Systems*. Prentice-Hall, Upper Saddle River, NJ.

Labar, C., Ebenbauer, C., and Marconi, L. (2022). Iss-like properties in lie-bracket approximations and application to extremum seeking. *Automatica*, 136, 110041.

Labar, C., Garone, E., Kinnaert, M., and Ebenbauer, C. (2019). Newton-based extremum seeking: A second-order lie bracket approximation approach. *Automatica*, 105, 356–367.

Leblanc, M. (1922). Sur l'électrification des chemins de fer au moyen de courants alternatifs de fréquence élevée. *Revue Générale de l'Électricité*, 12, 275–277.

Moase, W. and Manzie, C. (2012). Fast extremum-seeking for wiener-hammerstein plants. *Automatica*, 48, 2433–2443.

Moase, W., Manzie, C., and Brear, M. (2010). Newton-like extremum-seeking for the control of thermoacoustic instability. *IEEE Transactions on Automatic Control*, 55(9), 2094–2105.

Moreau, L. and Aeyels, D. (2000). Practical stability and stabilization. *IEEE Transactions on Automatic Control*, 45(8), 1554–1558.

Poveda, J.I. and Krstic, M. (2021). Non-smooth extremum seeking control with user-prescribed fixed-time convergence. *IEEE Transactions on Automatic Control*, 66(12), 6156–6163.

Scheinker, A. and Krstić, M. (2017). *Model-free stabilization by extremum seeking*. Springer.

Sontag, E.D. (1989). A 'universal'construction of artstein's theorem on nonlinear stabilization. *Systems & control letters*, 13(2), 117–123.

Tan, Y., Moase, W., Manzie, C., Nesic, D., and Mareels, I. (2010). Extremum seeking from 1922 to 2010. In *Proceedings of the 29th Chinese Control Conference*, 14–26.

Wang, H.H., Krstic, M., and Bastin, G. (1999). Optimizing bioreactors by extremum-seeking. *Int. J. Adaptive Control and Signal Processing*, 13, 651–669.